Image Processing Tool for Quantifying Immunostained Sections of Fibrotic Cardiac Tissue

A Capstone Report Submitted to the

Department of Biomedical Engineering

University of Virginia, Charlottesville, VA

In Partial Fulfillment of Requirements of the Degree

Bachelor of Science, School of Engineering

Jakub Lipowski

Spring, 2022

On my honor as a University Student, I have neither given nor received unauthorized aid on this assignment as defined by the Honor Guidelines for Thesis-Related Assignments

Signed_____Date 05/06/2022_____
Jakub Lipowski

Approved_____via email to Dr. Allen and Dr. Barker_____Date 05/06/2022_____
Shayn M. Peirce, Ph.D.

Number of Words: 4,177
Number of Figures: 6
Number of Tables: 0
Number of Equations: 0
Number of Supplements: 0
Number of References: 22

Image Processing Tool for Quantifying Immunostained Sections of Fibrotic Cardiac Tissue

Jakub Lipowski[a], Shayn M. Peirce[1]

[a] Undergraduate, Department of Biomedical Engineering, University of Virginia, Charlottesville, VA
[1] Correspondence: Shayn M. Peirce
email: jl5ef@virginia.edu, shayn@virginia.edu

Abstract

The inflammatory and wound healing process following myocardial infarctions causes an increase in populations of macrophages, fibroblasts, and monocytes in the tissue. Monocytes arrive at the infarct via perfused vessels and differentiate into macrophages, which in turn secrete cytokines that recruit fibroblasts to produce extracellular matrix proteins. The additional proteins stiffen the tissue, causing abnormal contractions during systole. We propose an image processing software that quickly identifies, labels, and counts ectodermal dysplasia 1 (ED1), ectodermal dysplasia 2 (ED2), alpha smooth muscle actin (αSMA;), and 4',6-Diamidino-2-Phenylindole (DAPI) positive cells to explore the dynamics of cell populations in the days following infarction. The purpose of this report is to describe the development of the image processing software rather than draw conclusions about the healing process following a myocardial infarction. A supervised machine learning pipeline was trained to identify ED1, ED2, αSMA, and DAPI stains. The image processing software was able to quantify cells across an entire tissue section as well as cells near key structures such as blood vessels. Three users were recruited to validate the software. Users counted cells manually and using the program. Analysis of variance tests showed that there was a significant difference between users' manual cell counts, but there was no difference between cell counts computed by the program. As a result, it was possible to conclude that the image processing tool was reliable. The outputs from this software can be used to inform future research in tissue engineering, especially multi-cell computational modeling.

Keywords: Myocardial infarction, immunostaining, image processing, machine learning, macrophage

Introduction

Nearly one third of all global deaths are a result of cardiovascular disease [1]. Of those deaths, 85 percent are caused by heart attacks and strokes, amounting to 15 million deaths annually [2]. The incidence rate is roughly 600 cases per 100,000 people [3]. Furthermore, the global economic burden onset by cardiovascular disease is expected to rise to 918 billion USD by 2030, which is nearly one percent of the current global gross domestic product [4]. As a result, it is important to develop a better understanding of heart attacks.

At the same time, about 45% of heart attacks are silent, meaning that damage is inflicted to the heart without the victim even knowing [5]. However, silent heart attacks can leave physical injuries in the form of scar tissue. Scar tissue

is fibrous tissue caused by injury. In the heart, fibrosis is particularly problematic because it can cause arrythmia, chamber dilation, and potentially heart failure [6]. In the case of heart attacks, 40 to 50 percent of people who die of one exhibit cardiac scar tissue, indicating that they have experienced a heart attack in the past [7].

The healing process following myocardial infarctions (MI), commonly referred to as a heart attack, consists of several multicell interactions. As a result, it is important to understand the dynamics between cell populations that play key roles in the healing process post-MI over time. However, spatiotemporal dynamics between cell populations are not well understood. What is understood, however, is that cardiomyocytes, monocytes, macrophages, and fibroblasts all play a role in the inflammatory response to MI. When cardiac tissue suffers a loss of blood flow, cardiomyocytes, cells responsible for producing the contractile force in the heart, produce an adrenergic response [8]. The adrenergic response is comprised of cardiomyocytes lowering the number and function of cardiac beta receptors, which causes a sympathetic response by altering downstream mechanisms [9]. One of these altered mechanisms causes an increase in the production of monocytes as a downstream result of activated bone marrow niche cells [10]. Once in the circulatory system, these monocytes arrive at the injured cardiac tissue via blood vessels. Meanwhile, monocytes differentiate into M1 macrophages and begin phagocytosing necrotic cells and secreting growth factors, including angiogenic ones such as vascular endothelial growth factor. Past research suggests that phagocytotic activity encourages M2 macrophage activation, which are resident macrophages [11]. M1 macrophages recruit fibroblasts, which secrete extracellular matrix proteins [12]. Secretion of protein causes the cardiac tissue to stiffen, which leads to the formation of scar tissue which increases susceptibility to arrythmia, chamber dilation, and potentially heart failure.

Developing a better understanding of the healing processing following MI is key to identification of therapeutic targets for enhanced cardiac tissue regenerations. Additionally, computational models are often used in the field of biology to quickly and inexpensively draw insights from virtual experiments. However, these models rely on accurate parameters used to model a given environment. A better idea of the spatiotemporal dynamics between cell types could lead to greater accuracies in parameterization of computational models that aim to study cardiac tissue fibrosis.

In the past, approaches have been taken to quantify the spatiotemporal dynamics of MI. One method used vectorcardiography, but this methodology does not offer insight into specific therapeutic interventions in terms of target cells [13]. Other studies have researched spatiotemporal dynamics among immune cells in MI, but produced more results pertaining to the signaling patterns between cells instead [14]. Using an image processing tool designed for analyzing sections of infarcted cardiac tissue from different timepoints following MI could offer a much more definite portrayal of spatiotemporal dynamics between the aforementioned cell types.

Image processing is an effective methodology to go about quantification of these cell populations. A widely accepted pipeline for the identification of objects in an image includes five steps: acquisition, filtering for noise reduction, segmentation, post-processing, and classification. Acquisition refers to obtaining images and ensuring a consistent standard of quality. Filtering for noise reduction is an important step in ensuring that data from images are interpretable. Segmentation is the process of dividing an image into disjoint regions. After an image is segmented, post-processing is implemented by filtering any remaining noise in the image. Lastly, classification refers to identifying artifacts in an image. A set of criteria need to be developed to objectively classify objects in an image [15]. Common criteria include pixel area, color, and shape. Machine learning can be used for the classification stage of any image processing pipeline. According to IBM, machine learning refers to computer algorithms that can improve automatically through experience [16]. Training a machine learning algorithm to identify objects in an image has potential to outperform human judgement.

It is hypothesized that the image processing tool will quantify cells more consistently than humans in addition to being much faster than humans. In order to develop a user-friendly image processing tool that could quantify cells across entire tissue sections and near key structures like blood vessels, three specific aims were set out for the project.

<u>Specific Aim #1:</u> To create a front-end, user-friendly graphical user interface along with a back-end supervised machine learning pipeline to process, identify, classify, and quantify cells in images of infarcted cardiac rat tissue.

<u>Specific Aim #2:</u> To complete validation of the image processing tool by recruiting users to count cells manually

and programmatically. Validation is necessary to ensure that the output of the software is reliable.

Specific Aim #3: To ensure that the software is open source by pushing all relevant code associated with the program to a public platform like GitHub. Ensuring an open source software leaves room for collaboration in the future.

Materials and Methods

Prior to development of the image processing tool, *in vitro* experiments were completed to obtain images of immunostained cardiac rat tissue. The completed image processing tool had two parts: a front-end user interface along with a back-end machine learning pipeline. The user interface was used to make analysis more user-friendly while the back-end machine learning pipeline was used to identify cells in images of immunostained cardiac tissue. Two analyses were developed for quantification of cell populations. A global analysis was used to quantify all cells across an entire tissue section while an annular analysis was used to quantify cell extravasation from blood vessels. Lastly, validation of the image processing tool was completed to ensure that the tool is reliable and consistent.

Obtaining images of immunostained cardiac rat tissue

Our collaborators at the University of Virginia's Department of Biomedical Engineering, Laura Caggiano, Ph.D. and Jeffrey Holmes, M.D., Ph.D., surgically induced MI into rats and removed the hearts at several timepoints following the injury. 21 rats were sacrificed. Three rats in the control group were healthy and did not suffer MI. There were six experimental groups, each consisting of three rats, that experienced surgically induced MI and were sacrificed one, two, three, four, five, and six days following MI. The rats were sacrificed in a carbon dioxide chamber and surgery was performed to remove the rat heart. The cardiac tissue was sectioned and immunostained. In this study, the only tissue sections that were considered came from the myocardium near the middle of the heart wall. Immunostaining was performed using three stains: ectodermal dysplasia 1 (ED1; M1 macrophage marker), ectodermal dysplasia 2 (ED2; M2 macrophage marker), alpha smooth muscle actin (αSMA; myofibroblast and vascular smooth muscle marker), and 4',6-Diamidino-2-Phenylindole (DAPI; nuclear marker) [17]–[19]. Montaged micrographs (about 12 mm by 11 mm in size) of entire immunostained cross-sections of cardiac tissue were obtained with a 10x objective using a Leica Thunder microscope. Figure 1 shows an image
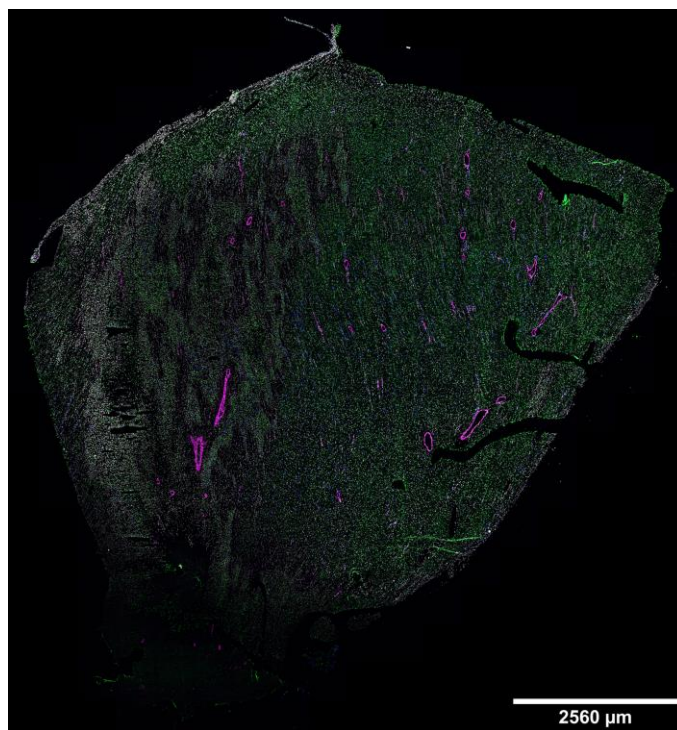

Fig. 1. Image of immunostained cardiac rat tissue. This image shows a cardiac tissue section taken from the myocardium. The tissue in this image suffered MI three days before the image was taken.

immunostained cardiac rat tissue that suffered MI four days before the image was taken.

Front-end user interface

A front-end GUI was developed to make the image processing tool user-friendly. Python (3.7) was used to develop this GUI. The GUI was divided into three panels, each with a different purpose and functionality in mind. The leftmost panel, panel 1, contains a "Browse" button that allows the user to parse through any directory on their computer to select an image of immunostained tissue. Once the image is selected, the middle panel, panel 2, displays the image. Panel 2 also includes user input fields. One field requires the user to select an immunostain of interest, either ED1 (M1 macrophage marker), ED2 (M2 macrophage marker), αSMA (myofibroblast and vascular smooth muscle marker), or DAPI (nuclear marker). The field above that requires the user to input the number of days that have elapsed following infarction of the imaged tissue. Another input field asks for the vessel identification number, which is useful organizational information when analyzing macrophage extravasation from blood vessels. The "Image Length" input field allows the user to specify the horizontal dimension of the image in microns. There are two buttons on the bottom of panel 2. The "Run Global Analysis" button

runs a program that computes data for the entire tissue section. The "Run Annular Analysis" button runs a program that opens another GUI so that the user may zoom in on any vessel in the image and compute macrophage extraversion. Once the analysis is complete, a schematized image of the annular analysis appears at the center of panel 2. Global and annular analyses are discussed in a latter portion of the methods and materials section. The user can press the "Reset" button to clear the current analysis and begin a new one. The rightmost panel, panel 3, outputs key statistics about the cell densities and counts computed by either the annular or global analyses. Lastly, all data that is entered into panel 2 and output to panel 3 is recorded in an Excel spreadsheet. Figure 2 depicts the GUI along with the three referenced panels that comprise it. Packages used to make the GUI included PySimpleGUI, PIL, io, pandas, and openpyxl.

Back-end machine learning pipeline

A back-end machine learning pipeline was implemented to identify different cells in images of immunostained cardiac rat tissue. The first step of the supervised machine learning pipeline was to clean the data and reduce noise. Since each image was about a gigabyte in size, these images were reduced to 25% of their original size on the Leica Thunder computer to make analysis less computationally expensive. Each resized image was divided into 81 smaller image tiles to make analysis less intensive, computationally speaking. Ilastik (1.4.0b5), Python-based program used for image analysis, was used for image segmentation. Cells were distinguishable based on the RGB pixel value in the image,
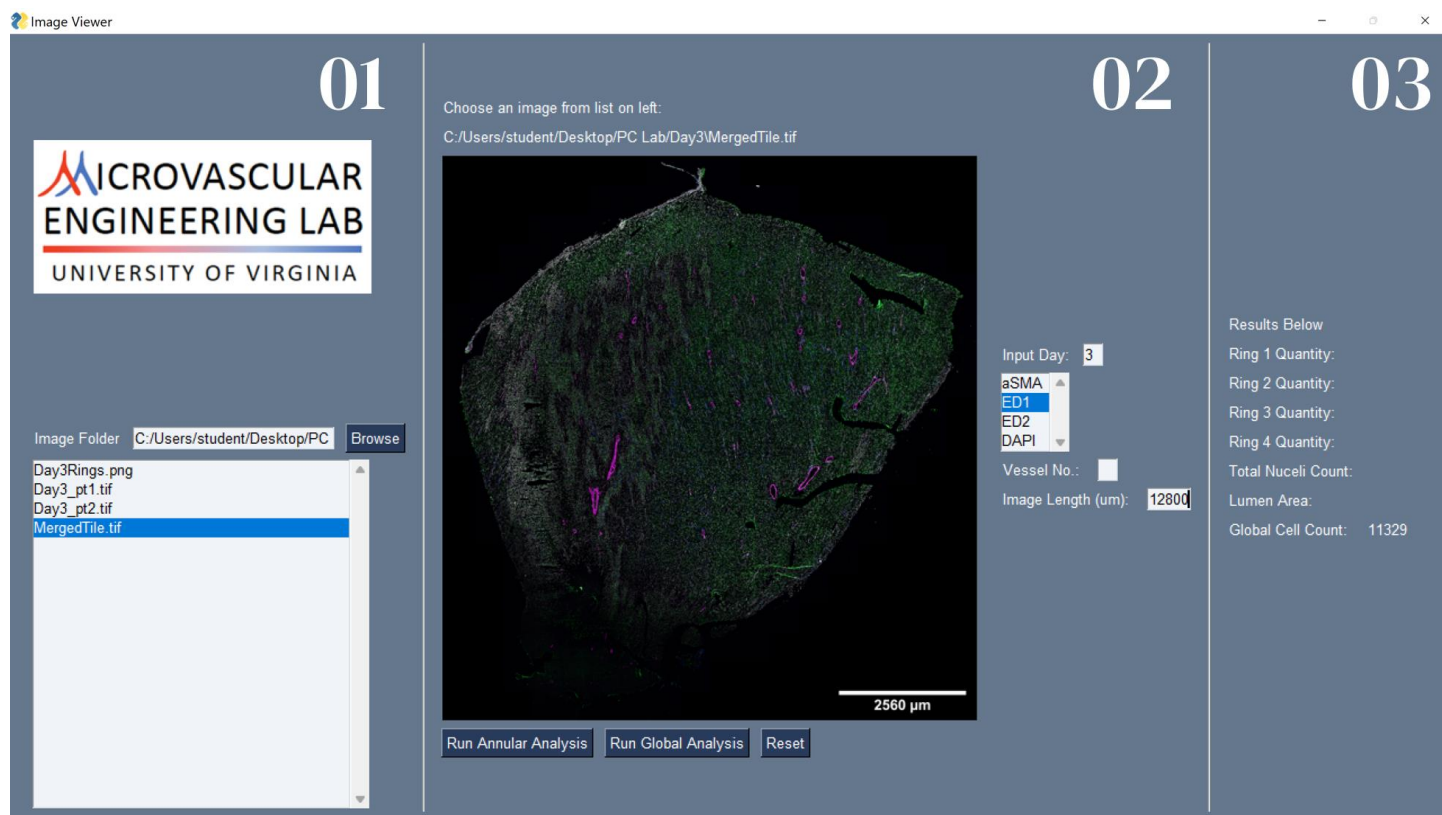

Fig. 2. Front-end graphical user interface. The user interface is divided into three panels. Panel 1 is used to identify an image that will be analyzed. Panel 2 is used to perform analysis. Panel 3 shows preliminary output. A comprehensive output is written to an Excel spreadsheet.

analogous to the color of the corresponding immunostain, the brightness of each pixel, and the number of similar pixels adjacent to each other. As the "golden standard" for the machine learning algorithm, a human identified certain pixels within an image and assigned the label of ED1+, ED2+, αSMA+, or DAPI+ to the object. In addition, everything else that was not a cell type of interest in the labeling process was labeled as background. These human-identified artifacts were the training data. Four image tiles were used to train the machine learning algorithm for each stain. Classifications of data obtained from this "golden standard" were generalized to other images so that all the cells within the image could be labeled as ED1+, ED2+, αSMA+, or DAPI+ cells. Once training was completed, all images were run through Ilastik to identify cell populations. For each image, all 81 tiles were pushed through the algorithm. For each tile, the output from the machine learning algorithm was a binary, black and white image. In these images, white pixels corresponded to cells while black pixels corresponded to everything that was not a cell. Figure 3 depicts an image tile along with the output from the machine learning pipeline.
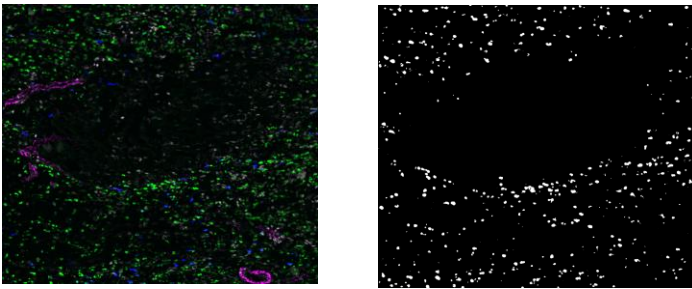

Fig. 3. Supervised machine learning pipeline input and output. The image on the left shows an image tile taken from a rat that was sacrificed four days post-MI. The image on the right shows the output from the supervised machine learning model that was used to identify ED1+ cells (M1 macrophages) which are green in the image on the left.

After all 81 tiles were processed for an image, the tiles were stitched back together to form a complete, binary image identifying cells in white pixels and everything else in black pixels.

Program functionality: global analysis

Global analysis was developed in Python to count cells across entire tissue sections. A program was written that counted the total number of cells in the image. To achieve this a binary, black and white image was analyzed. Since there were only two colors in the image, the program was able to count the number of white objects in the image. An object was defined as any continuous region in the image comprised of white pixels. The perimeter of each white object was calculated. Any objects that had an area of less than five pixels were disregarded and were assumed to be noise in the data because these objects were too small to be cells. Next, the centroid of each object was computed. It was assumed that one centroid corresponded to one cell. Operating under this assumption, the total number of cells in a tissue section was determined by the number of centroids in the image.

Program functionality: annular analysis

Annular analysis computed cell extravasation from blood vessels. Once the user opted to perform annular analysis by clicking the "Run Annular Analysis" button on the GUI, a second GUI appeared displaying the full image. Next, the user could zoom in on a blood vessel. Blood vessels were identified by pink/red circular structures. αSMA, which appeared pink/red, stains for vascular smooth muscle cells which comprise the blood vessel walls, making identification of blood vessels relatively simple. Once the user selected a blood vessel, the user was prompted to trace the exterior of the blood vessel. This could be done with a finger or stylus on a touch screen device or a computer mouse. Once the vessel was traced, the program computed four concentric rings radiating away from the vessel. The diameter of each ring increased by two times the diameter of the traced blood vessel. Next, the cells in each annular region were quantified by computing the centroids of cells in the image and only included the ones in a specific annular region. These cell counts, divided by the area of the annular regions, yielded the cell density in the three annular regions. The cell densities and counts in the lumen of the blood vessel and three annular regions were written to an Excel spreadsheet along with the date that the data was collected. Additionally, an image of the immunostained blood vessel and surrounding tissue along with a schematized interpretation of annular analysis were saved to a specified directory and displayed on the middle panel of the GUI. The schematized interpretation of annular analysis shows cells as points on a plot and the annular regions are outlined with circular curves. Figure 4 shows the schematized interpretation of the annular analysis performed on a blood vessel.

Packages used to create the two functionalities included PIL, numpy, cv2, math, shapely, matplotlib, and datetime.
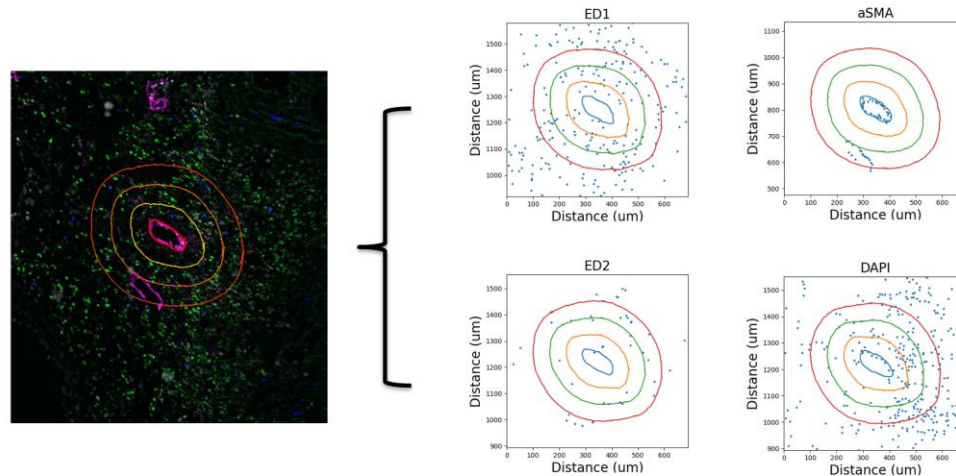
Fig. 4. Description of annular analysis. The image of the left shows a blood vessel after the user outlines it and the program computes the perimeters of annular regions. The four images on the right show the schematized interpretations of the annular analysis. The blue dots represent identified cells and the circular curves correspond to the perimeters of annular regions defined in the image of immunostained tissue. The title of each plot corresponds to the stain type that the blue dots represent.

Validation of image processing tool

Three users were recruited to validate the image processing tool. Each user was tasked with two forms of analysis: manual and automated analysis. Manual analysis required each user to perform annular analysis on specified blood vessels. The user would manually count the number of cells in each annular region near the blood vessel. The automated analysis required users to perform the annular analysis on the same blood vessel using the software, meaning that the data of interest was the one output by the image processing tool. Users were instructed to perform this analysis on 179 blood vessels. To ensure that each user performed the analysis the same as other users, all users were instructed on how to complete the analysis using video instructions. Statistical tests were performed to determine whether the software was consistent and reliable.

Making code publicly available

Finally, all code used to develop the image processing tool was pushed to GitHub. The code is open source and can be downloaded, used, or altered by anyone. A brief user manual is also included, instructing users how to run the image processing tool. Users may access the repository using at: https://github.com/KubaLipowski/Capstone.git.

Results

Validation results

A series of t-tests and two analysis of variance (ANOVA) tests were performed to determine that the image processing tool is reliable. Three users obtained manual and automated cell counts by performing annular analysis for 179 vessels.

For each vessel, users obtained cell counts for ED1+, ED2+, αSMA+, and DAPI+ cells. The two-tailed, paired t-tests compared each individual user's manual cell counts to automated cell counts for each individual stain. At a significance level of 0.05, it was determined that 75% of the time the p-value was high, meaning that there was no statistically significant difference between the manual cell counts and the automated cell counts. Two two-factor, without replication ANOVA tests compared the three users against each other. One ANOVA test was used to compare the manual cell counts, while the other was used to compare the automated cell counts. A significance level of 0.05 was adopted for both tests. The test comparing manual cell counts resulted in a p-value of 0.00, meaning that there was a significant difference between manual cell counts among the three users. The test comparing automated cell counts resulted in a p-value of 0.08, meaning that there was not a significant difference between automated cell counts.

Image processing results

The image processing tool developed preliminary insights into the healing process following MI. Global analysis was performed on each of the images coming form rats in the control group and all the experimental groups. It was determined the number of M1 macrophages over time steadily increased, while the number of M2 macrophages remains relatively constant during the healing process following MI. Figure 5 demonstrates this relationship.
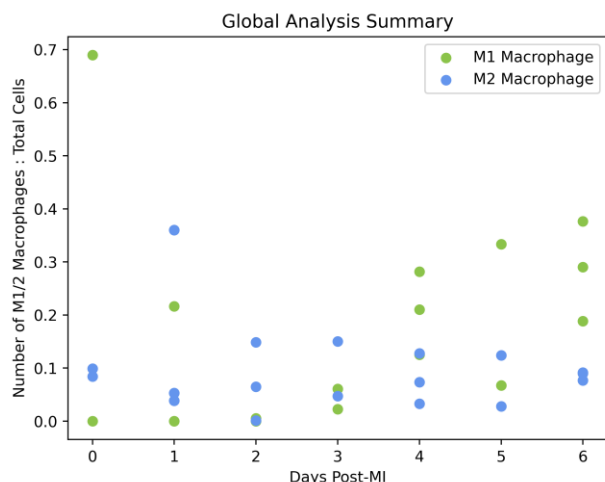
Fig. 5. Global analysis summary. Each M1 macrophage is represented by a green point, while each M2 macrophage is represented by a blue point. All macrophage counts were divided by the total number of cells in the tissue section. 'Day 0' refers to the control group of healthy rats. Days 1, 3, and 5 include only two samples per cell type because these images had too much noise.

Annular analysis was used to visualize cell extravasation from blood vessels. Cell densities for M1 macrophages (ED1+ cells), M2 macrophages (ED2+ cells), and fibroblasts and vascular smooth muscle cells (αSMA+ cells) were collected and averaged from several annular regions surrounding blood vessels. Figure 6 depicts a visualization of annular analysis over several timepoints following MI.

Discussion

Advantages of the image processing tool

The statistical analyses have shown that the image processing tool is consistent across independent runs of the software. The t-tests comparing manual and automated counts for each user for each cell type yielded a p-value higher than 0.05 75% of the time. Generally, users agreed with the program's output. The ANOVA test comparing manual counts computed by three different users had a p-value below 0.05, demonstrating that human users did not produce consistent results when counting cells manually. The second ANOVA test comparing automated cell counts obtained by each user produced a p-value above 0.05, demonstrating that the program was consistent no matter who used it. Additionally, the software was able to save researchers time when quantifying cell populations. There were expected to be between 20,000 to 30,000 nuclei identified by DAPI (stained for all nuclei) markers alone within each individual image. Making the generous
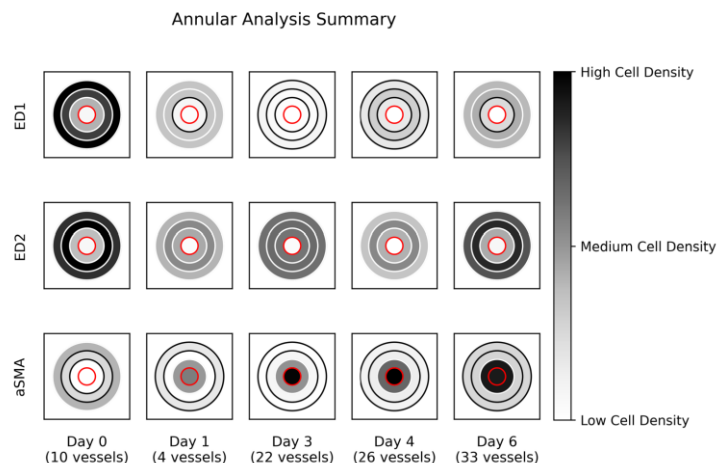

Fig. 6. Annular analysis summary. The red circle in the middle of each plot represents a blood vessel. The annuli surrounding each vessel correspond to annular regions. The shading of each annulus, representing cell density. is relative to other shades of annuli in the same row. Therefore, shadings of annuli in different rows are independent of each other. Days 2 and 5 were omitted because not enough large blood vessels were visible in the images that were collected.

assumption that a human is able to count one nucleus per second, it would take anywhere between 5.55 to 8.33 hours to count the nuclei in a single image. However, the image processing tool can quantify all these cells in less than three seconds.

Preliminary insights about MI

Based on the global analysis and annular analysis insights, it is hypothesized that M1 macrophages initially arrive at the scene of the infarct via blood vessels, but then increase their population by proliferation. This hypothesis explains the steady increase in M1 macrophage populations over time in the global analysis along with the initial high cell density of ED1+ cells near blood vessels, followed by a decrease in cell density in the annular analysis. It makes sense that the M2 macrophage population is relatively stable over time because M2 macrophages are resident macrophages, so they are always on site. No strong conclusions could be drawn about fibroblast populations because much of the αSMA+ cells computed were vascular smooth muscle cells comprising blood vessel walls.

Existing cell quantification tools

Three common existing tools for cell quantification are ImageJ, the hemocytometer, and the Corning Cell Counter. ImageJ is a free image processing tool made available by the NIH. For the purposes of cell counting, it provides two

main functionalities: thresholding and a manual cell counting tool [20]. Thresholding is not reliable because it solely relies on pixels' RGB values causing several artifacts in an image that are not truly cells to slip through the threshold. A hemocytometer is generally used for blood samples and is not equipped with the latest visualization technologies [21]. The Corning Cell Counter is more accurate than a hemocytometer, but is very expensive, with prices as high as $8,000 [22]. Therefore, it made sense to develop an open-source image processing tool to quickly and inexpensively quantify large cell populations. No software products exist for annular analysis of blood vessels. To our knowledge, no image processing software currently exists for the purpose of analyzing extraversion of cells from blood vessels. Since monocytes arrive at the region of the infarct via perfused blood vessels, it is important to quantify cell populations within the vicinity of these key structures.

Limitations

The front-end GUI and the back-end machine learning pipeline were disjoint, meaning that users must push all images through the machine learning pipeline and save outputs to a specified directory before analyzing the images using the GUI. Another limitation was that the back-end machine learning pipeline was only adapted to immunostained images. Other stains, such as hemoxylin and eosin or picrosirius stains, were not covered by the image processing tool. Lastly, when an image had several cells within close proximity to each other, the fluorescent label made it challenging to distinguish individual cells. Occasionally, the classification algorithm would consider a clump of cells as one large cell. Although this resulted in an underestimate of total number of cells, the naked eye would also struggle to distinguish the number of cells in these fluorescent clusters. During the development of the image processing tool, images from only the myocardium were used. However, to get a more complete analysis of the healing process post-MI, images from other regions of the heart wall need to be included as well. Lastly, it was difficult to distinguish which αSMA+ stain corresponded to vascular smooth muscle cells and fibroblasts, making analysis of these cell types less meaningful.

Implications for future work

Next steps for the image processing program are based around developing a user community to improve the software. Now that the code is pushed to GitHub, researchers have the opportunity to edit the software as they see fit. This includes adding functionalities to the software

to quantify image properties or editing existing functionalities. Another important step for future work would be to train the machine learning algorithm to identify other types of stains. The infrastructure for the machine learning is already there, it is just a matter of training the algorithm to identify cells in new images. For the purposes of studying the healing process post-MI, it is necessary to obtain images from the endocardium and epicardium to develop a more complete understanding of the healing process follow MI. Ultimately, a peer review board will need to review the image processing tool to ensure its credibility by publishing in a journal in the future.

Conclusion

The image processing tool detailed in this report is versatile, scalable, and can be adapted easily to contexts outside of MI. By way of automation, the image processing tool saves researchers time during the data collection phase of research, allowing for quick generation of hypotheses and conclusions that drive research initiatives forward. The image processing tool introduced a novel annular analysis, which can help uncover spatiotemporal dynamics between cell populations in MI. Results output from this image processing tool can be applied to preliminary steps in studies within the emerging fields of regenerative medicine and computational modeling to help identify targets for enhanced regeneration and parameterization of models, respectively.

End Matter

References

[1] "Cardiovascular diseases." https://www.who.int/health-topics/cardiovascular-diseases (accessed May 03, 2022).

[2] "Cardiovascular diseases (CVDs)." https://www.who.int/news-room/fact-sheets/detail/cardiovascular-diseases-(cvds) (accessed May 03, 2022).

[3] D. K. Arnett *et al.*, "2019 ACC/AHA Guideline on the Primary Prevention of Cardiovascular Disease: A Report of the American College of Cardiology/American Heart Association Task Force on Clinical Practice Guidelines," *Circulation*, vol. 140, no. 11, Sep. 2019, doi: 10.1161/CIR.0000000000000678.

[4] J. G. Travers, F. A. Kamal, J. Robbins, K. E. Yutzey, and B. C. Blaxall, "Cardiac Fibrosis," *Circ. Res.*, vol. 118, no. 6, pp. 1021–1040, Mar. 2016, doi: 10.1161/CIRCRESAHA.115.306565.

[5] "The danger of 'silent' heart attacks," *Harvard Health*, Jan. 01, 2017. https://www.health.harvard.edu/heart-health/the-danger-of-silent-heart-attacks (accessed May 03, 2022).

[6] "What role does scar tissue play in recovery from heart disease? | Imperial News | Imperial College London." https://www.imperial.ac.uk/news/174206/what-role-does-scar-tissue-play/ (accessed May 03, 2022).

[7] J. Howard, "Many sudden cardiac deaths linked to prior silent heart attacks, study says," *CNN*, Jul. 10, 2019. https://www.cnn.com/2019/07/10/health/heart-attack-sudden-cardiac-death-study/index.html (accessed May 03, 2022).

[8] P. Dutta and M. Nahrendorf, "Monocytes in Myocardial Infarction," *Arterioscler. Thromb. Vasc. Biol.*, vol. 35, no. 5, pp. 1066–1070, May 2015, doi: 10.1161/ATVBAHA.114.304652.

[9] M. J. Lohse, S. Engelhardt, and T. Eschenhagen, "What Is the Role of β-Adrenergic Signaling in Heart Failure?," *Circ. Res.*, vol. 93, no. 10, pp. 896–906, Nov. 2003, doi: 10.1161/01.RES.0000102042.83024.CA.

[10] P. Dutta *et al.*, "Myocardial infarction accelerates atherosclerosis," *Nature*, vol. 487, no. 7407, pp. 325–329, Jul. 2012, doi: 10.1038/nature11260.

[11] J. M. Lambert, E. F. Lopez, and M. L. Lindsey, "Macrophage Roles Following Myocardial Infarction," *Int. J. Cardiol.*, vol. 130, no. 2, pp. 147–158, Nov. 2008, doi: 10.1016/j.ijcard.2008.04.059.

[12] A. V. Shinde and N. G. Frangogiannis, "Fibroblasts in myocardial infarction: a role in inflammation and repair," *J. Mol. Cell. Cardiol.*, vol. 70, pp. 74–82, May 2014, doi: 10.1016/j.yjmcc.2013.11.015.

[13] H. Yang, S. T. S. Bukkapatnam, T. Le, and R. Komanduri, "Identification of myocardial infarction (MI) using spatio-temporal heart dynamics," *Med. Eng. Phys.*, vol. 34, no. 4, pp. 485–497, May 2012, doi: 10.1016/j.medengphy.2011.08.009.

[14] A. T. Bejjani, S. A. Saab, D. H. Muhieddine, N. J. Habeichi, G. W. Booz, and F. A. Zouein, "Spatiotemporal Dynamics of Immune Cells in Early Left Ventricular Remodeling After Acute Myocardial Infarction in Mice.," *J. Cardiovasc. Pharmacol.*, Nov. 2019, doi: 10.1097/fjc.0000000000000777.

[15] "Image Processing Methods for Automatic Cell Counting In Vivo or In Situ Using 3D Confocal Microscopy | IntechOpen." https://www.intechopen.com/chapters/18389 (accessed May 03, 2022).

[16] "What is Machine Learning? | IBM." https://www.ibm.com/cloud/learn/machine-learning (accessed May 03, 2022).

[17] Bio-Rad, "ED Clone Antibodies for Studying Rat Macrophage Subtype Markers & Related Molecules," *Bio-Rad*. https://www.bio-rad-antibodies.com/ed-clone-antibodies-for-rat-macrophage.html (accessed Nov. 07, 2021).

[18] B. Hinz, G. Celetta, J. J. Tomasek, G. Gabbiani, and C. Chaponnier, "Alpha-Smooth Muscle Actin Expression Upregulates Fibroblast Contractile Activity," *Mol. Biol. Cell*, vol. 12, no. 9, pp. 2730–2741, Sep. 2001.

[19] B. I. Tarnowski, F. G. Spinale, and J. H. Nicholson, "DAPI as a useful stain for nuclear quantitation," *Biotech. Histochem. Off. Publ. Biol. Stain Comm.*, vol. 66, no. 6, pp. 297–302, 1991.

[20] I. V. Grishagin, "Automatic cell counting with ImageJ," *Anal. Biochem.*, vol. 473, pp. 63–65, Mar. 2015, doi: 10.1016/j.ab.2014.12.007.

[21] "Common Challenges of Cell Counting with a Hemocytometer," *DeNovix*, Apr. 27, 2020. https://www.denovix.com/blog/challenges-cell-counting-hemocytometer/ (accessed Nov. 07, 2021).

[22] "Thomas Scientific Corning Cell Counter - Corning Cell Counter, 200x Magnification - 1159B191 Each / Each," *Grayline Medical*. https://www.graylinemedical.com/products/thomas-scientific-corning-cell-counter-corning-cell-counter-200x-magnification-1159b19 (accessed Nov. 07, 2021).